Tuning the Structure of Ultrathin $BaTiO_3$ Films on Me(001) (Me = Fe, Pd, Pt) Surfaces

H. L. Meyerheim,[1,*] A. Ernst,[1,5,†] K. Mohseni,[1] I. V. Maznichenko,[2] J. Henk,[2] S. Ostanin,[1] N. Jedrecy,[3] F. Klimenta,[1] J. Zegenhagen,[4] C. Schlueter,[4] I. Mertig,[1,2] and J. Kirschner[1,2]

[1]*Max-Planck-Institut für Mikrostrukturphysik, Weinberg 2, D-06120 Halle, Germany*
[2]*Institut für Physik, Martin-Luther-Universität Halle-Wittenberg, D-06099 Halle, Germany*
[3]*Institut des Nano Sciences de Paris, UPMC-Sorbonne Universités, CNRS-UMR7588, 75005 Paris, France*
[4]*ESRF, Boîte Postale 220, F-38043 Grenoble Cedex, France*
[5]*Wilhelm-Ostwald-Institut für Physikalische und Theoretische Chemie, Universität Leipzig, Linnéstraße 2, 04103 Leipzig, Germany*

(Received 25 November 2012; revised manuscript received 1 March 2013; published 4 September 2013)

Using surface x-ray diffraction in combination with *ab initio* calculations, we demonstrate that the atomic structure of ultrathin $BaTiO_3$ (BTO) films grown on Me(001) surfaces (Me = Fe, Pd, Pt) depends on subtle modifications of the interface chemical composition. A complete reversal of the surface termination from a BaO- [BTO on Fe(001)] to a TiO_2-terminated film [BTO on Pt(001)] is observed which goes in parallel with the adsorption of submonolayer amounts of oxygen at metal hollow sites of the interface. Our results may suggest a new route to an overall control of both the surface and the interface geometry in $BaTiO_3$/metal contacts.

DOI: 10.1103/PhysRevLett.111.105501 PACS numbers: 61.05.cp, 68.35.Ct, 68.47.Gh, 77.55.fe

The metal-oxide interface is at the heart of novel oxide functional nanoscale devices, in which the barrier between the metallic electrodes is composed of a ferroelectric or multiferroic material. Polarization reversal of the ferroelectric tunnel barrier leads to a change of the tunneling conductance [1,2], mediated by the interface atomic geometry and the internal electronic potential [3–6].

Since a well-defined and stable interface structure is decisive for the device properties, thermodynamic stability of the ferroelectric barrier and high-quality controlled growth on the metal electrodes is a prerequisite. Recent experimental studies have given evidence that ultrathin $BaTiO_3$ (BTO) layers can be grown on Fe(001) [7] and vice versa [8], leading to well-defined coherent interfaces essential for ballistic tunneling. Owing to the intimate relation between interface atomic geometry and the tunneling properties, the proper design of both the barrier atomic structure and its interface to the electrodes are of the utmost importance. So far, however, neither experimental nor theoretical evidence exists with regard to the stability of the two most simple BTO/Me interface configurations, namely, TiO_2/Me or BaO/Me, as well as its consequences on the overall film structure and the tunneling properties.

Moreover, calculations for the perovskite-type BTO barrier [4,5,9] generally assume symmetric structures with identical (TiO_2) terminations to the metal electrodes; however, experimental evidence obtained for films in the ultrathin limit ($\approx$ 1–3 unit cells) does not support this assumption [7]. For instance, BTO grows in complete unit cells, leading to a $[BaO/TiO_2]_n$/Me structure characterized by a BaO-terminated film surface. Furthermore, theory in general assumes perfect interfaces between BTO and the metal, i.e., excluding any kind of structural defects and/or chemical contaminations in the surface structure or at the interface between BTO and the metal, which are difficult to detect by conventional surface analytical tools. Consequently, the analysis of the detailed atomic structure including subtle chemical and structural defects and their effect on the barrier is mandatory; however, systematic studies of the atomic interface have not been reported.

To this end, we have carried out surface x-ray diffraction (SXRD) experiments to analyze different BTO/Me(001) (Me = Fe, Pd, Pt) interface structures. We find that subtle modifications of the interfacial chemistry involve a transition from a BaO-terminated film surface (on Fe) to a TiO_2-terminated film surface (on Pt).

Experiments were carried out at the beam line ID32 of the European Synchrotron Radiation Facility in Grenoble (France). The films were grown *in situ* under ultrahigh vacuum conditions by pulsed laser deposition (PLD) using a stoichiometric BTO target, followed by annealing up to 550 °C to obtain a long-range-ordered structure. After deposition, film thickness and stoichiometry were controlled by Auger electron spectroscopy. We have studied films of nominally two unit cell thickness on different substrates: (i) Fe(001), (ii) Pt(001), and (iii) Pd(001), on which BTO with a bulk lattice constant of $a = 3.991$ Å grows fully strained with a low lattice misfit of $\varepsilon = +1.7\%$, -1.8%, and -2.5%, respectively. These values are related to the centered settings of the metal-surface unit cells. For all films, a $c(2 \times 2)$ low energy electron diffraction pattern is observed with respect to the primitive surface unit cell.

SXRD data were collected under grazing incidence using x rays at a wavelength of $\lambda = 0.55$ Å. The total integrated intensity $I(hk\ell) \propto |F_{\mathrm{tot}}(hk\ell)|^2$ can be expressed by the interference sum of the bulk and surface contributions: $|F_{\mathrm{tot}}(hk\ell)|^2 = |F_B(hk\ell) + F_S(hk\ell)\exp[i\phi]|^2$. Here, F_B represents the structure factor of the bulk crystal

truncation rod (CTR) at integer-order positions (h, k) in reciprocal space [10,11], while F_S corresponds to the surface contribution at integer- and fractional-order positions [12]. Because of the truncation of the crystal, the third coordinate ℓ becomes a continuous parameter. The interference of F_B and F_S allows the determination of the registry between bulk and surface structures, formally expressed by the phase factor $\exp[i\phi]$.

As a representative example, Fig. 1 shows the magnitudes of experimental (symbols) and calculated (lines) structure factors ($|F_{\mathrm{tot}}|$) for BTO/Pd(001). Both integer-order CTRs and half-order superlattice rods are shown. For the latter, only a smooth sinusoidal variation of $|F_{\mathrm{tot}}(hk\ell)|$ as a function of ℓ is observed. This is due to the absence of F_B at the fractional-order positions [12]. Along the CTRs bulk Bragg reflections appear at $\ell = 2n - (h + k)$ for CTRs (n integer).

For all samples discussed in this study, the structure analysis was carried out by first constructing start models, assuming configurations with different interface and surface terminations, and simultaneously optimizing the fractional coverage of the TiO_2 and the BaO layers. As will be discussed below, this provided a detailed insight into the different surface terminations (pure BaO, mixed TiO_2/BaO, and pure TiO_2) which are characteristic for the BTO films grown on Fe, Pd, and Pt, respectively. In a second step, the z positions of the atoms (including the first two substrate layers) were refined by least squares refinement of the calculated $|F_{\mathrm{tot}}|$ to the experimental ones. We benefit from the high $p4mm$ plane group symmetry of the structure, allowing the x and y positions of the atoms to be kept fixed. Figure 1 shows two calculations based on the $BaO/TiO_2/BaO/TiO_2/Pd(001)$ (solid black line) and the $TiO_2/BaO/TiO_2/BaO/Pd(001)$ (dashed red line) structure. The fit quality is quantified by the unweighted residuum R_u and the goodness of fit (GOF) [13]. For the first model, R_u and GOF are equal to 10% and 1.5%, respectively. For the second model R_u is in the 30%–40% range (GOF = 4.8), clearly indicating that the first model with the TiO_2 interface layer shown in Fig. 2(c) is the correct one. More details concerning the SXRD analysis are reported in the Supplemental Material [14].

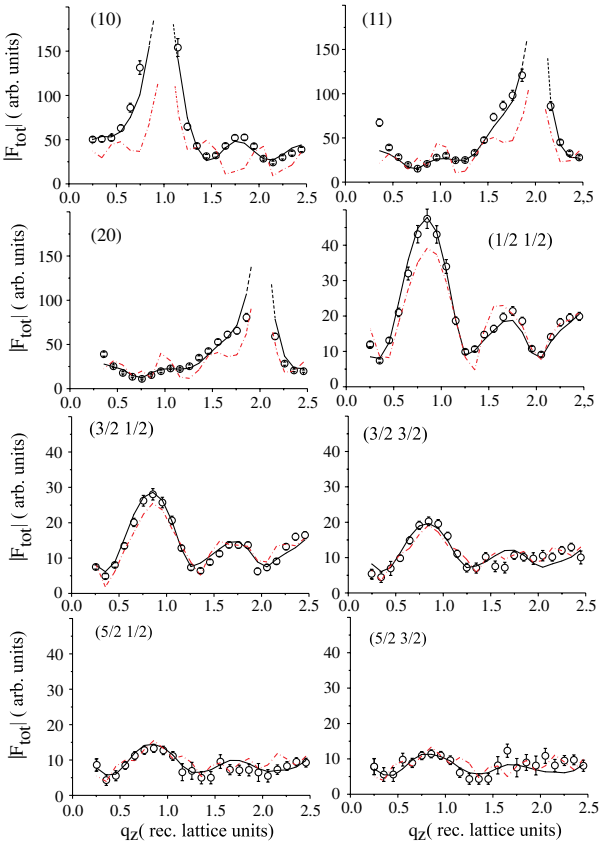

FIG. 1 (color online). Experimental (symbols) and calculated (lines) structure factor amplitudes for BTO on Pd(001). Note the different y-axis scales for superlattice rods (half order) and crystal truncation rods (integer order). Solid (black) and dashed (red) lines correspond to calculated $|F_{\mathrm{tot}}|$'s, assuming a TiO_2 and a BaO layer at the interface to Pd(001) (see the text).

Figure 2 shows the structure models derived from the SXRD analysis for the four different types of samples: (a) BTO/Fe(001), (b) $BTO/Fe(001)_{(C)}$, (c) BTO/Pd(001), and (d) BTO/Pt(001). In the case of (b), BTO was grown on a Fe(001) surface which was intentionally "contaminated" by carbon before deposition [labeled by $Fe(001)_{(C)}$]. The presence of carbon was proven by Auger electron spectroscopy and by the observation of a diffuse $c(2 \times 2)$ low energy electron diffraction pattern. It should be noted that in the structure models, the number of atoms in each layer approximately represents the (relative) occupancy, but not island sizes, which for PLD grown films of this thickness are considerably larger ($\approx$ 20 nm) than a few unit cells.

Experimental results and their interpretations are supported by first-principles calculations using the VASP code, well known for its precise determination of energies and forces [15,16]. The structures were modeled within a slab geometry, using a nine-monolayer-thick substrate supercell covered on top with the ferroelectric films of a given thickness. A 2-nm-thick vacuum layer separates the slabs along [001]. The calculations were carried out within the generalized gradient approximation of density functional theory [17]. The most important results can be summarized as follows.

(i) In all films (Fe, Pd, Pt), the SXRD analysis clearly shows that BTO grows with a TiO_2 layer in contact with the metal surface. This geometry, in which the oxygen atoms are located on top of the metal atoms at distances of 1.75 Å (BTO/Fe), 1.64 Å ($BTO/Fe_{(C)}$), 2.30 Å (BTO/Pd), and 2.50 Å (BTO/Pt), allows the formation of a metal-oxygen bond. Experimental uncertainties for the distance determination lie in the 0.05–0.10 Å range. First-principles calculations reveal that the TiO_2/Me interface is energetically preferred as compared to the formation of the

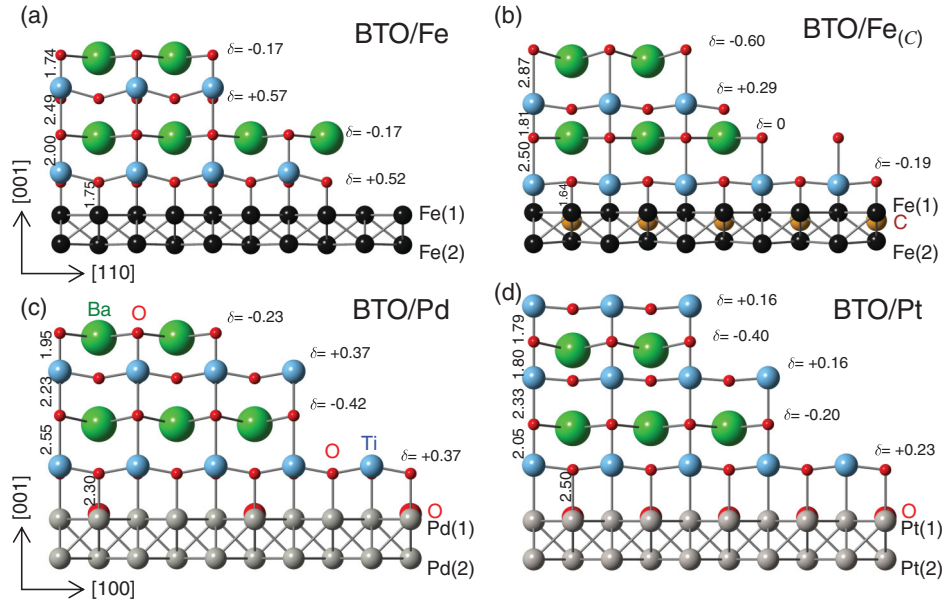

FIG. 2 (color). Structure models for ultrathin BTO films grown on metal substrates: (a) BTO/Fe, (b) BTO/$Fe_{(C)}$, (c) BTO/Pd, and (d) BTO/Pt. Small (red), large (green), and medium sized (blue) spheres represent oxygen, barium, and titanium atoms, respectively. Numbers represent distances in Ångstrom, and the parameter δ indicates the vertical shift of the cation above ($\delta > 0$) or below ($\delta < 0$) the level of oxygen atoms. Fractional coverage of a layer is qualitatively indicated by the number of spheres in the layers relative to that in the substrate.

BaO/Me interface. For the BTO/Fe interface, the energy preference defined by $\Delta E = E([\mathrm{BaO/TiO_2}]_n/\mathrm{Fe}) - E([\mathrm{TiO_2/BaO}]_n/\mathrm{Fe})$ equals -2.0 eV, while we find for BTO/Pd $\Delta E = -0.54$ eV and for BTO/Pt $\Delta E = -0.50$ eV. The large ΔE in the case of BTO/Fe is due to the strong Fe-O bond at the interface. In Fig. 3(a), the high charge density (red circles) between oxygen and the Fe atoms indicates a strong covalent bond. By contrast, in the case of the hypothetical BaO/Fe interface [Fig. 3(b)], the Fe-O distance is substantially larger than in the case of the TiO_2/Fe interface (2.05 Å vs 1.75 Å) that leads to a much weaker Fe-O bonding. For the BTO/Pd and BTO/Pt films, the energy gain is less than a quarter of that in the BTO/Fe case, indicating a weaker bonding between the substrate and oxygen atoms of the adjacent TiO_2 layer. This can be related to the respective metal work functions (Φ), which in the case of Fe ($\Phi = 4.60$ eV) [18] is smaller than in the cases of Pd ($\Phi = 5.10$ eV) and Pt ($\Phi = 5.65$ eV).

For BTO/Fe, the calculation of the Fe-O distance (1.65 Å) is in fair agreement with experiment (1.75 Å). By contrast, for Pd-O (2.00 Å) and Pt-O (2.10 Å), the calculated distances are too small by 0.30 and 0.40 Å, respectively. This mismatch is resolved by taking into account the experimentally detected presence of interface oxygen. Including interfacial oxygen into the calculations leads to Pd-O and Pt-O distances of 2.37 and 2.50 Å, respectively, in very good agreement with experiment.

(ii) In parallel with the increasing metal-oxygen distance along the sequence BTO/Fe→BTO/Pd→BTO/Pt, there is an increasing concentration of interfacial oxygen located in the fourfold hollow sites. In the following, the concentration (θ) is given in monolayers (ML), where one ML refers to one adsorbate atom per substrate atom. We find $(\theta) \approx 0$ for BTO/Fe, but $(\theta) = 0.25$ ML for BTO/Pd and $(\theta) = 0.50$ ML for BTO/Pt [uncertainties for the determination of (θ) lie in the 0.1 ML range]. Oxygen atoms are located in one of two symmetry-independent hollow sites within the $c(2 \times 2)$ reconstructed surface unit cell, here below the second layer Ba atom. For the oxygen-Pt (Pd) distances, we derive 1.97 Å

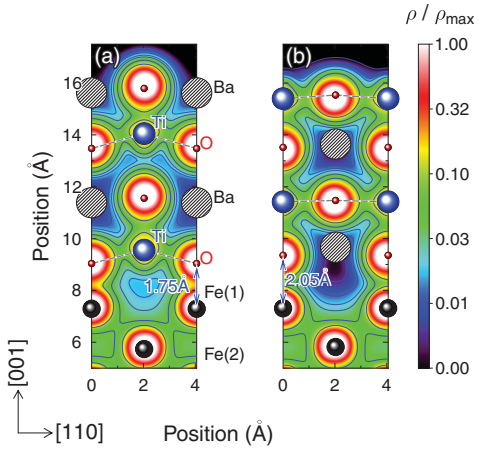

FIG. 3 (color). Calculated charge densities and interatomic distances for BTO/Fe(001) assuming different interface structures: (a) TiO_2/Fe and (b) BaO/Fe. Atoms are represented by spheres as in Fig. 2; Ba atoms (hatched circles) are not located in the depicted plane.

(1.98 Å) along the in-plane and 2.11 Å (2.23 Å) along the perpendicular direction, respectively. We suggest that the presence of interfacial oxygen is related to an excess of oxygen generated by the PLD process.

The limited amount [$(\theta) \leq 0.1$ ML] of interfacial oxygen at the BTO/Fe interface is attributed to steric reasons: The short Fe-O bond and the corresponding low vertical distance between the interfacial TiO_2 layer and the top Fe layer excludes the presence of interfacial oxygen despite its chemical affinity to Fe. By contrast, the smaller carbon atom can adsorb in the hollow site. Because of its low scattering cross section, an accurate determination of the carbon position is impossible.

(iii) The modification of the interface chemical composition from 0.00 to 0.50 ML of oxygen induces a reversal of the surface termination to the vacuum: While the BTO film on Fe is entirely terminated by BaO [Fig. 2(a)], a pure TiO_2 termination is found for BTO/Pt [Fig. 2(d)]. Correspondingly, an intermediate situation is observed for BTO/Pd, which is characterized by a mixed TiO_2/BaO termination [Fig. 2(c)]. It is important to note that a mixed TiO_2/BaO termination is found for BTO/$Fe_{(C)}$ as well [Fig. 2(b)]. This observation provides direct evidence that the interfacial chemical composition influences the film termination: Its decisive role can be related to the condition of charge neutrality within the whole film. In the case of BTO/Fe, the interface is free from adsorbed species and BTO grows in complete unit cells [7]. Since the BTO interface to the metal is characterized by a TiO_2 layer, the surface is terminated by a BaO layer, in this way preserving charge neutrality of the whole system. An adsorbed species at the interface involves an alteration of the charge distribution within the whole film, leading to a modification of the surface terminating layer.

(iv) Finally, we comment on some more details of the film structure, which is controlled by both the choice of the substrate and the interfacial chemistry. From the values of the parameter δ, which represents the vertical shift between the cation and the oxygen atoms in each layer (see Fig. 2), it is clear that the sequence within the film is in general $(+, -, +, \ldots)$ for the (TiO_2, BaO, $TiO_2, \ldots$) layers, respectively. In bulk BTO, δ for TiO_2 (δ_{TiO_2}) equals ± 0.11 Å at room temperature. In comparison, values derived for the ultrathin films are substantially larger, indicating a strong (lateral) strain-driven ($\Delta a/a = \varepsilon$) increase of the polarization. The impact of strain on the polarization of BTO films is discussed in detail in the Supplemental Material [14].

(v) To estimate the impact of the interfacial structure on the transport properties in a M/BTO/M (M = Fe, Pd, Pt) tunnel junction, we calculated the z-resolved charge density at the Fermi level integrated over the 2D unit cell [$\rho(E_F)$] using a self-consistent Green function method designed especially for semi-infinite layered systems [19]. According to the results of the structure analysis,

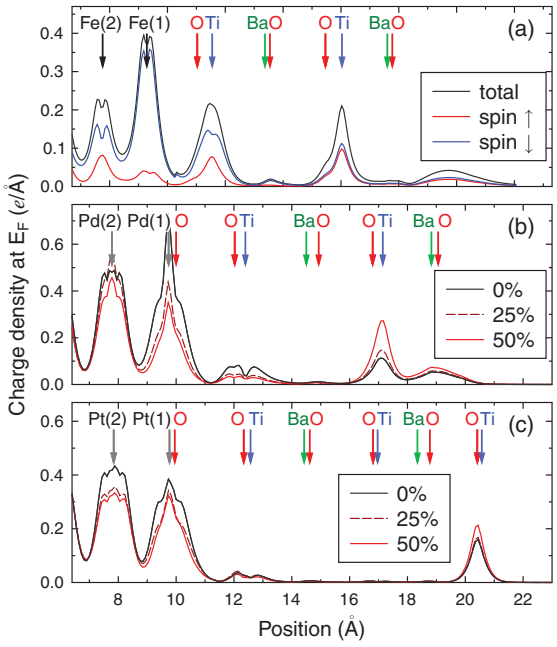

FIG. 4 (color). Z-resolved charge distribution calculated at the Fermi level for (a) BTO/Fe, (b) BTO/Pd, and (c) BTO/Pt films. In the case of BTO/Fe, the spin-resolved and the total charge distribution are shown; in the case of BTO/Pd and BTO/Pt, the different lines correspond to calculations assuming 0.00, 0.25, and 0.50 ML of oxygen at the interface (see labels). Arrows indicate the atomic positions taken from the structure analysis.

the interfacial oxidation in the case of BTO/Pd and BTO/Pt was taken into account and simulated for three occupancies (θ): $\theta = 0$ ML (pure case), $\theta = 0.25$ ML, and $\theta = 0.50$ ML. The results are shown in Fig. 4.

For all films, there is clear evidence for metallization of the film surface. Depending on the substrate metal (Fe, Pd, Pt)—and thus on the surface termination—there is a continuous variation of $\rho(E_F)$, from "more delocalized" in the case of the BaO film termination [Fig. 4(a)] to "localized" at the TiO_2 termination [Fig. 4(c)]. Also, $\rho(E_F)$ in the vicinity of the interface strongly depends on the structural and chemical details. Most importantly, $\rho(E_F)$ is spin polarized in BTO/Fe [Fig. 4(a)], with the minority spin charge being dominant at the interface. The strong bonding between the oxygen atoms and the Fe substrate results in an enhancement of $\rho(E_F)$ in the first TiO_2 layer, which is distinctly different from the BTO/Pd [Fig. 4(b)] and the BTO/Pt interface [Fig. 4(c)].

In accordance with Refs. [20,21], we find that the metal layers and the BTO layers are mostly coupled by electronic states with Δ_1 symmetry (i.e., s, p_z, and d_{z^2} orbitals). These states are of particular importance for coherent transport because they provide efficient transport channels [22–24]. It should be emphasized that from Fig. 4, it is obvious that in the case of BTO/Pd and BTO/Pt, the partial oxidation has only a minor effect on $\rho(E_F)$. Thus, one might speculate that the coherent transport would

be marginally affected as well, which is at variance with the well-investigated tunneling magnetoresistance system Fe/MgO/Fe, where it was shown that even small amounts of oxygen can strongly reduce the tunneling magnetoresistance ratio [25,26].

In summary, we have presented a combined surface x-ray diffraction and theoretical study of the atomic geometry in ultrathin $BaTiO_3$ films deposited on (001) oriented metal surfaces of Fe, Pd, and Pt. We find that subtle changes of the interface chemical composition characterized by the presence of only 0.25–0.50 ML of oxygen or carbon substantially modify the atomic film geometry involving changes in the vertical atomic positions and—most importantly—leading to a reversal of the film-surface termination from BaO (BTO/Fe) to TiO_2 (BTO/Pt). Owing to the decisive role of the interface geometry in perovskite-based oxide (multiferroic) tunnel junctions, our results may open a new route for the design of suitable barriers in general.

We (H. L. M., F. K., and N. J.) thank the staff of the European Synchrotron Radiation Facility for their hospitality during our stay in Grenoble. Help during experiments by S. Förster is gratefully appreciated. We thank F. Weiss for technical support. This work is supported by the DFG through SFB 762.

*hmeyerhm@mpi-halle.de
†aernst@mpi-halle.de

[1] W. Eerenstein, N. D. Mathur, and J. F. Scott, Nature (London) **442**, 759 (2006).
[2] E. Y. Tsymbal and H. Kohlstedt, Science **313**, 181 (2006).
[3] M. Y. Zhuravlev, R. F. Sabirianov, S. S. Jaswal, and E. Y. Tsymbal, Phys. Rev. Lett. **94**, 246802 (2005).
[4] J. P. Velev, C.-G. Duan, K. D. Belashchenko, S. S. Jaswal, and E. Y. Tsymbal, Phys. Rev. Lett. **98**, 137201 (2007).
[5] J. P. Velev, C.-G. Duan, K. D. Belashchenko, S. S. Jaswal, and E. Y. Tsymbal, J. Appl. Phys. **103**, 07A701 (2008).
[6] M. Fechner, I. V. Maznichenko, S. Ostanin, A. Ernst, J. Henk, P. Bruno, and I. Mertig, Phys. Rev. B **78**, 212406 (2008).
[7] H. L. Meyerheim, F. Klimenta, A. Ernst, K. Mohseni, S. Ostanin, M. Fechner, S. Parihar, I. V. Maznichenko, I. Mertig, and J. Kirschner, Phys. Rev. Lett. **106**, 087203 (2011).
[8] L. Bocher, A. Gloter, A. Crassous, V. Garcia, K. March, A. Zobelli, S. Valencia, S. Enouz-Vedrenne, X. Moya, N. D. Marthur *et al.*, Nano Lett. **12**, 376 (2012).
[9] M. Stengel, D. Vanderbilt, and N. A. Spaldin, Nat. Mater. **8**, 392 (2009).
[10] I. K. Robinson, Phys. Rev. B **33**, 3830 (1986).
[11] R. Feidenhans'l, Surf. Sci. Rep. **10**, 105 (1989).
[12] E. Vlieg, J. V. D. Veen, S. Gurman, C. Norris, and J. Macdonald, Surf. Sci. **210**, 301 (1989).
[13] The unweighted residual is defined as $R_u = \sum ||F^{\mathrm{obs}}| - |F^{\mathrm{calc}}|| / \sum |F^{\mathrm{obs}}|$. GOF is defined by $\mathrm{GOF} = \sqrt{1/(N-P)\sum[(|F^{\mathrm{obs}}| - |F^{\mathrm{calc}}|)^2/\sigma^2]}$. Here, F^{obs} and F^{calc} are the experimental and calculated structure factors, respectively, while N and P represent the number of data points and the number of refined parameters. The parameter σ represents the standard deviation of F^{obs}. The summation runs over all data points.
[14] See Supplemental Material at http://link.aps.org/supplemental/10.1103/PhysRevLett.111.105501 for x-ray analysis of the film and interface structure.
[15] G. Kresse and J. Furthmüller, Phys. Rev. B **54**, 11 169 (1996).
[16] J. Hafner, J. Comput. Chem. **29**, 2044 (2008).
[17] J. P. Perdew, K. Burke, and M. Ernzerhof, Phys. Rev. Lett. **77**, 3865 (1996).
[18] H. B. Michaelson, J. Appl. Phys. **48**, 4729 (1977).
[19] M. Lüders, A. Ernst, W. M. Temmerman, Z. Szotek, and P. J. Durham, J. Phys. Condens. Matter **13**, 8587 (2001).
[20] W. H. Butler, X.-G. Zhang, T. C. Schulthess, and J. M. MacLaren, Phys. Rev. B **63**, 054416 (2001).
[21] S. S. P. Parkin, C. Kaiser, A. Panchula, P. M. Rice, B. Hughes, M. Samant, and S.-H. Yang, Nat. Mater. **3**, 862 (2004).
[22] C. Tusche, H. L. Meyerheim, N. Jedrecy, G. Renaud, A. Ernst, J. Henk, P. Bruno, and J. Kirschner, Phys. Rev. Lett. **95**, 176101 (2005).
[23] C. Tusche, H. L. Meyerheim, N. Jedrecy, G. Renaud, A. Ernst, J. Henk, P. Bruno, and J. Kirschner, Phys. Rev. Lett. **96**, 119602 (2006).
[24] P. Bose, P. Zahn, I. Mertig, and J. Henk, Phys. Rev. B **83**, 174451 (2011).
[25] X.-G. Zhang, W. H. Butler, and A. Bandyopadhyay, Phys. Rev. B **68**, 092402 (2003).
[26] P. Bose, A. Ernst, I. Mertig, and J. Henk, Phys. Rev. B **78**, 092403 (2008).